



Can land degradation drive differences in the C exchange of two similar semiarid ecosystems?

Ana López-Ballesteros^{1,2}, Cecilio Oyonarte^{3,4}, Andrew S. Kowalski^{5,6}, Penélope Serrano-Ortiz^{1,6}, Enrique P. Sánchez-Cañete^{5,6,7}, M. Rosario Moya², Francisco Domingo²

- 5 ¹Departamento de Ecología, Universidad de Granada, Granada, 18071, Spain
²Departamento de Desertificación y Geo-ecología, Estación Experimental de Zonas Áridas (CSIC), Almería, 04120, Spain
³Departamento de Agronomía, Universidad de Almería, Almería, 04120, Spain
⁴Centro Andaluz de Evaluación y Seguimiento del Cambio Global (CAESCG). Universidad de Almería. Almería, 04120, Spain
10 ⁵Departamento de Física Aplicada, Universidad de Granada, Granada, 18071, Spain
⁶Instituto Interuniversitario de Investigación del Sistema Tierra en Andalucía (IISTA-CEAMA), Universidad de Granada, Granada, 18006, Spain
⁷B2 Earthscience, Biosphere 2, University of Arizona, Tucson, Arizona, 85721, USA
- 15 *Correspondence to:* Ana López-Ballesteros (alpzballesteros@gmail.com)

Abstract. The concept of land degradation stems from the loss of an ecosystem's biological productivity, which in turn relies on several degradation processes, such as long-term loss of natural vegetation, depletion of soil nutrients, soil compaction or water and wind erosion, to which drylands are especially vulnerable. Currently, drylands occupy more than one third of the global terrestrial surface and will probably expand under future climate change scenarios. Drylands' key role in the global C balance has been recently demonstrated, but the effects of land degradation on C sequestration by these ecosystems needs further research. In the present study, we compare net carbon exchange, together with satellite data and meteorological, ambient and vadose zone (CO₂, water content and temperature) variables, between two nearby (~23 km) experimental sites representing "natural" (i.e. site of reference) and "degraded" grazed semiarid grasslands located in SE Spain, via eddy covariance measurements over 6 years, with highly variable precipitation magnitude and distribution. Results show a striking difference in the annual C balances with an average release of 196 ± 40 and -23 ± 20 g C m⁻² yr⁻¹ for the "degraded" and "natural" sites, respectively. At the seasonal scale, differing patterns in net CO₂ fluxes were detected over both growing and dry seasons. As expected, during the growing seasons, greater net C uptake over longer periods was observed in the "natural" site, however, much greater net C release was measured in the "degraded" site during drought periods. We tested differences in all monitored meteorological and soil variables and found it most relevant that CO₂ at 1.50 m belowground was around 1000 ppm higher in the "degraded" site. Thus, we believe that subterranean ventilation of this vadose zone CO₂, previously observed at both sites, largely drives the differences in C dynamics between them, especially during the dry season maybe due to enhanced subsoil-atmosphere interconnectivity in the "degraded" site. Overall, the 12 site-years of data allow direct exploration of the roles of climate and land degradation in the biological and non-biological processes that ultimately control the C sequestration capacity of semiarid ecosystems.



1 Introduction

The concept of land degradation stems from the loss of an ecosystem's biological productivity, which in turn relies on several degradation processes such as long-term loss of natural vegetation, deterioration of soil quality, depletion in biodiversity or water and wind erosion (UNCCD, 1994). Arid, semiarid and dry sub-humid areas, commonly known as drylands, have been recognized as areas vulnerable to land degradation processes. Overall, drylands occupy more than one third of Earth's land surface and are inhabited by more than 2 billion people (Niemeijer et al., 2005), and concretely, the semiarid ecoregion comprises a major fraction, 37% of global dryland area, where the dominant biome is grassland (Niemeijer et al., 2005). Drylands have expanded globally for the last sixty years at an estimated annual rate of 5.8 million hectares in mid latitudes alone (Lal, 2001), and are projected to expand under future climate change scenarios (Feng and Fu, 2013; Cook et al., 2014). Furthermore, the Mediterranean region has been recognized as an especially vulnerable region (Gao and Giorgi, 2008), where major expansions of semiarid areas will occur (Feng and Fu, 2013).

Over recent decades, most research focused on land degradation has been based on remote sensing and earth observation techniques. Much of these investigations has aimed to refine methodological issues in order to accurately track land degradation in vulnerable areas, reduce uncertainties and explain inconsistencies among studies. For instance, a wide array of satellite-derived data, such as vegetation indices, normalized surface reflectance, brightness temperature or biomass-net primary production derivatives (Mbow et al., 2015), has been utilized to appraise desertification effects in the Sahel (Mbow et al., 2015; Fensholt et al., 2013) and also in other African countries such as Kenya (Omuto, 2011), Somalia (Omuto et al., 2010), South Africa (Thompson et al., 2009) or Zimbabwe (Prince et al., 2009). Likewise, desertification in the Mediterranean region has been studied through satellite imagery, concretely, in Greece (Bajocco et al., 2012), Israel (Shoshany and Karnibad, 2015) and the Iberian Peninsula (del Barrio et al., 2010). Additionally, some global assessments based on modelling approaches have focused on the global loss of net primary production derived from land degradation (Zika and Erb, 2009) or the effect of desertification on climate (Wang et al., 2016). However, although drylands' key role in the global carbon (C) balance has been demonstrated (Poulter et al., 2014; Ahlström et al., 2015), very few investigations have directly quantified how land degradation processes disturb the C sequestration capacity of drylands (Lal, 2001), which is one of the most important ecosystem services (Watanabe and Ortega, 2011).

In this regard, the few C-related desertification studies conducted over last decade have centred on soil C dynamics. Concretely, soil organic carbon (SOC) inventories have been used to explore the effects of climate, human activities and grazing pressure in desertification-prone areas of China (Feng et al., 2006) and Brazil (Schulz et al., 2016). Similarly, other investigations have evaluated soil degradation processes by means of soil CO₂ effluxes together with other biometric measurements in drylands found in China (Hou et al., 2014; Wang et al., 2007), Chile (Bown et al., 2014) and southeast Spain (Rey et al., 2011; Rey et al., 2017). However, the degradation processes associated with desertification affect several subsystems as well as their interactions at multi- spatial and temporal scales. For instance, adverse effects on soil quality involve depletion of soil fertility, but also reduce soil-water storage (Mainguet and Da Silva, 1998), which, in turn, can



constrain seed germination and vegetation reestablishment, modify climax vegetation, disrupt biogeochemical cycles, alter water and energy balances, and consequently lead to a loss of ecosystem resilience (Lal, 2001). This cascade of disturbances may result in a reduction of the C sequestration capacity of a given ecosystem, which is clearly a symptom of the loss of biological productivity, resulting in a positive feedback to global warming. Therefore, a quite suitable and holistic approach is to integrate all subsystems effects into a whole ecosystem-scale assessment when quantifying the C loss derived from land degradation. However, the use of this integrative method is mostly lacking in the available literature.

The present study is located in an area, the southeast of Spain, that has been recognized as a hotspot of land degradation owing to the synergistic interaction of sociological and climatic factors (Puigdefábregas and Mendizabal, 1998), where, furthermore, rainfall has trended downward at ca. 3 mm yr⁻¹ since 1900 (Oñate-Rubalcaba, 1993). Our core aim is to evaluate how dryland degradation affects the dynamics of net ecosystem-atmosphere C exchange of two semiarid grasslands that represent differing degradation status by means of meteorological and satellite measurements, subsoil CO₂ sensors and the eddy covariance (EC) technique (Baldocchi et al., 1988). This technique allows us to directly quantify the net exchange of energy, water and CO₂ flux densities (hereinafter fluxes) between an ecosystem (including all of its subsystems, i.e. soil, plants, microorganism, vadose zone...) and the atmosphere at a high frequency (from minutes to hours). Owing to the high temporal resolution of the EC method, we can assess the effect of land degradation as a slow change or disturbance legacy in the studied ecosystems and how, in turn, it influences the capacity of these ecosystems to absorb fast changes or short-term disturbances, such as droughts. Accordingly, our main hypothesis is that the degree of land-degradation affects net ecosystem C sequestration capacity through its impact on some or all of the processes that compose the overall ecosystem C balance: photosynthesis, ecosystem respiration (biological processes) and subterranean ventilation – a non-biological process that provokes the transfer of CO₂-rich air from subsoil to atmosphere under drought and high turbulence conditions. In this context, as subterranean ventilation has been measured in both experimental sites (Rey et al., 2012; López-Ballesteros et al., 2017), we also hypothesize a significant role of this process in the monitored ecosystems. Hence, our specific objectives are: (1) to compare C sequestration capacity of two semiarid ecosystems showing a differing degradation status, (2) to study involved processes (biological vs non-biological) and influencing factors that can drive potential differences in the net C exchange of studied ecosystems, and (3) to evaluate whether degradation can modulate ecosystem responses against short-term disturbances. To do this, we analysed 12 site-years of EC data, Enhanced Vegetation Index (EVI) time series and monitored ambient variables registered over the same period (2009-2015) at both sites. Additionally, we used subsoil CO₂, moisture and temperature data obtained during 2014-2015.

2 Material and Methods

30 2.1 Experimental sites description

The study area is located in southeast Spain, the driest part of Europe. The two experimental sites, Amoladeras (N36°50'5''W2°15'1'') and Balsa Blanca (N36°56'26.0'' W2°01'58.8''), are found within the Cabo de Gata-Níjar Natural



Park (Almería, Spain; Fig. 1) and are quite similar in terms of climate and ecosystem type. Both sites show a desert climate, according to Köppen classification (Bwh; Kottek et al., 2006), with a mean annual temperature of 18°C, mean annual precipitation of approximately 220 mm.

The ecosystem type corresponds to *espartal*, a Mediterranean semiarid grassland where the dominant species is *Machrocloa tenacissima*. This ecosystem type is widely extended over the Western Mediterranean region, in fact, in Cabo de Gata-Níjar Natural Park, a great fraction of agricultural areas that were abandoned over 1957-1994 resulted in *espartal* ecosystems (Alados et al., 2011; Alados et al., 2004). The functioning of both experimental sites can be divided into two main periods. On one hand, the growing season usually extends from late autumn to early spring, when the temperature starts to rise and water resources have not yet become scarce (López-Ballesteros et al., 2016; Serrano-Ortiz et al., 2014). On the other hand, a long period of hydric stress, with high temperatures and scarce precipitation, results in a prolonged dry season that usually begins in May-June and ends in September-October, when the first autumn rainfall events occur. Additionally, water inputs derived from relevant dewfall episodes, which have been previously reported (Uclés et al., 2014) in the area, can rehydrate soil and plants during night and early morning hours.

Regarding the topographic, geologic and edaphic characteristics, both sites are located on an alluvial fan, where the main geological materials consist of quaternary conglomerates and Neogene-Quaternary sediments cemented by lime (caliche) (Rodríguez-Fernández et al., 2015) and slopes of 2-6% (Rey et al., 2017) so no significant runoff occurs. Additionally, both sites present petrocalcic horizons. However, altitude and soil type differ. While Balsa Blanca (hereinafter BB) is located at an altitude of 208 m and has MollicLithic Leptosols (Calcaric), Amoladeras (hereinafter AMO) is situated closer to sea level, at 65 m, and presents less developed soils Lithic Leptosol (Calcaric; Table 1).

Overall, as stated by Rey et al. (2011), these two experimental sites represent different degradation stages owing to their differing soil characteristics and surface fractions (Table 1). While BB has more deep and fertile soils and higher vegetation cover, AMO shows thinner and poorer soils and has half of Balsa Blanca's vegetation cover. Therefore, in accordance to Rey et al. (2011; 2017), we considered that BB represents the “natural” site, being, currently, a representative ecosystem of the area, while AMO represents a “degraded” site with respect to BB.

2.2 Meteorological and eddy covariance measurements

The net ecosystem-atmosphere exchange of water vapour, CO₂ and sensible and latent heat were measured in terms of fluxes via the eddy covariance (EC) technique. Thus, an EC station was installed at each experimental site, AMO and BB (with site codes “Es-Amo” and “Es-Agu” of the European Database Cluster <http://www.europe-fluxdata.eu>), where ambient and micrometeorological variables (detailed in Table 2) were monitored continuously since 2009. The EC footprint (i.e. actual measured area) is well within the fetch (i.e. distance to a change in surface characteristics) at both sites. Regarding data processing, the half-hourly averaged fluxes were calculated from raw data collected at 10 Hz using EddyPro 5.1.1 software (Li-Cor, Inc., USA). Flux calculation, flux corrections and quality assessment were performed according to López-Ballesteros et al. (2016).



Additionally, flux measurements acquired under low-turbulence conditions were excluded from the analysis by using a friction velocity (u_*) threshold according to the approach proposed by Reichstein et al. (2005). The average u_* thresholds for the whole study period (i.e. 2009–2015) were 0.11 and 0.16 m s^{-1} , for AMO and BB, respectively. Furthermore, over the six years of measurements at both sites, data gaps due to low-turbulence conditions, instrument malfunction and theft were unavoidable and not randomly distributed, as noted by Ma et al. (2016). Therefore, the total annual fractions of missing half-hourly net CO_2 fluxes accounted for $33 \pm 3 \%$ and $29 \pm 6 \%$ of night-time data and $8 \pm 6 \%$ and $14 \pm 5 \%$ of day-time data, for AMO and BB, respectively. Missing data were gap-filled by means of the marginal distribution approach proposed by Reichstein et al. (2005) and errors derived from the gap-filling procedure were calculated from the variance of the gap-filled data, as explained by López-Ballesteros et al. (2016). The annual cumulative C balance was estimated, when possible, by integrating gap-filled half-hourly net CO_2 fluxes of good quality (0 and 1 quality flags, according to Mauder and Foken, 2004) over a hydrological year.

In order to test the validity of both EC stations, we assessed the energy balance closure (Moncrieff et al., 1997) by computing the linear regression of half-hourly turbulent energy fluxes, sensible and latent heat fluxes ($H+LE$; W m^{-2}) against available energy, net radiation less the soil heat flux (R_n-G ; W m^{-2}) with the whole six-years database. The resulting slopes were 0.873 ± 0.002 ($R^2 = 0.907$) and 0.875 ± 0.001 ($R^2 = 0.920$) for AMO and BB, respectively.

2.3 Enhanced Vegetation Index data series

We used Enhanced Vegetation Index (EVI) data acquired by the Moderate Resolution Imaging Spectroradiometer (MODIS), which is on board the Earth Observing System-Terra platform, in order to track vegetation dynamics at both experimental sites. The nominal resolution of EVI products (code “MOD13Q1”) is 250 m at nadir and temporal resolution corresponds to 16-day compositing periods. The spatial coordinates used for AMO and BB were $\text{N}36.8340^\circ$, $\text{E}2.2526^\circ$ and $\text{N}36.9394^\circ$, $\text{E}2.0341^\circ$, respectively. The EVI is a three-band vegetation index encompassing blue, red and NIR spectral reflectance information and has been widely used to track temporal variation of vegetation structure (Gao et al., 2000).

2.4 Vadose zone measurements

Subsoil CO_2 molar fraction, temperature and volumetric water content were measured at 0.05 m and 1.50 m below the surface (Table 2) from January 2014 to August 2015 at both experimental sites. In the case of the shallower CO_2 sensor, it was installed vertically with an in-soil adapter (211921GM, Vaisala, Inc., Finland) to avoid water entrance. Subsoil CO_2 molar fractions were sampled every 30 s and 5 min averages were stored in a data logger (CR3000 and CR1000, CSI; for AMO and BB, respectively). The deeper CO_2 sensor was equipped with a soil adapter for horizontal positioning (215519, Vaisala, Inc., Finland), consisting of a PTFE filter to protect to the CO_2 sensor from water. It was buried in the summer of 2013 and the measurements were made every 30 s and stored as 5 min averages in a datalogger (CR1000 and CR23X Campbell Sci., Logan, UT, USA, for AMO and BB, respectively). All CO_2 molar fraction records were corrected for variations in soil temperature and atmospheric pressure.



2.6 Statistical analysis

All meteorological and soil variables monitored at each site were compared through computation of the non-parametric two-sided Wilcoxon summed rank test in order to detect those factors/variables influencing potentially distinct ecosystem functioning between sites. This test was chosen because variables used satisfied the independence and continuity assumptions but not all were normally distributed. The confidence level used was 95% and the effect size was evaluated using an estimator based on confidence intervals that corresponded to the median of the difference between the samples (Amoladeras minus Balsa Blanca) and was expressed as an absolute value (Diff) and as a standardized value (Diff_{st}; dimensionless), which was obtained by using the sample values of every site divided by its standard deviation in order to be able to compare results among different variables. This analysis was performed by using three different periods: the whole study period, the period from May to September and the period from May to September during only daytime. These periods were selected given their demonstrated coincidence with high relevance of non-biological processes. All calculations were performed using R software version 3.2.5.

Additionally, in order to include the relationship between pressure and subsoil CO₂ variations as a potential factor influencing net CO₂ exchange (Sánchez-Cañete et al., 2013), we firstly calculated, separately for each site, Spearman correlation coefficients to determine the time step (6, 12, 24 or 72 hours) with the highest correlation between the differential transformation of pressure and the subsoil CO₂ molar fraction at 1.50 m.

3 Results

3.1 Ambient conditions over the study period

Over the study period, the wettest hydrological year was 2009/2010, with annual precipitation of ~500 mm (ca. twice the annual average precipitation for both sites over the study period, Fig. 2). On the contrary, the driest year was 2013/2014, with annual precipitation of ~100 mm for both sites, less than half the annual average precipitation registered at Amoladeras (AMO) and Balsa Blanca (BB). Generally, the months with precipitation higher than 20 mm occurred from the beginning of autumn until midwinter, however, in case of 2009/2010, 2010/2011, 2012/2013 and 2014/2015, relevant precipitation events were registered during spring months. By contrast, in 2013/2014, precipitation was always below 20 mm with the exception of November and December, for both sites, and June, in the case of AMO (Fig. 2a). Commonly, while maximum precipitation usually occurred from November to February, there was a remarkable drought period over summer months (June-August) when it scarcely ever rained (Fig. 2).

Regarding air temperature (T_{air}) patterns, monthly averaged T_{air} ranged from 9.6 and 8.1 °C to 27.6 and 27.9 °C in AMO and BB, respectively, over the entire study period. Based on half-hourly averaged data, minimum and maximum T_{air} values registered were 0.1 and 37.9 °C in AMO, and -1.3 and 39.9 °C, in BB, respectively. On one hand, those months with T_{air} above 15 °C usually corresponded to April-November, approximately. Additionally, August was the month with the highest



average T_{air} at both sites, with T_{air} ranges of 25.2 - 27.6 °C at AMO and 24.9 - 27.9 °C at BB, respectively (Fig. 2), over the study period. On the other hand, the lowest monthly average T_{air} usually occurred in January but sometimes also in December and February, with 11.2 – 12.3 °C at AMO and 8.1 - 14.1 °C at BB.

3.2 Annual carbon balances

5 The comparison of the annual carbon (C) balance among sites was only possible for three hydrological years, 2009/2010, 2010/2011 and 2012/2013, due to long-term data gaps existing in BB during other years. The annual cumulative net CO₂ exchange was always positive for AMO (i.e., net C release), whereas BB was neutral or even acted as a C sink over the three years (Fig. 3). For example, in 2009/2010, the net C uptake measured in BB equated to $32 \pm 10 \text{ g C m}^{-2}$ while in AMO, a total amount of $185 \pm 10 \text{ g C m}^{-2}$ was released to the atmosphere (Fig. 3a). The year with the largest difference between sites
10 was 2010/2011, with annual C release of 240 ± 8 and $-38 \pm 10 \text{ g C m}^{-2}$ in AMO and BB, respectively (Fig. 3b). Likewise, 2011/2012 was the year when the lowest CO₂ release was measured in AMO with $163 \pm 7 \text{ g C m}^{-2}$ while a neutral C balance was measured in BB with $0 \pm 8 \text{ g C m}^{-2}$ (Fig. 3c).

Overall, a positive and saturating trend was observed at both sites during autumn months until December-February when cumulative net CO₂ release start to decline. The autumn net CO₂ release (i.e., positive values) was usually higher in AMO
15 than in BB, excepting for 2012/2013, and the declining slope was always higher in BB, meaning greater net C uptake rates. Although the pattern of the cumulative net CO₂ exchange showed differences between sites over autumn, winter and spring months, stronger discrepancies were found during summer droughts. Concretely, from April-May until August, BB showed neutral behavior while a remarkable positive trend was observed in AMO, denoting a large net CO₂ release.

3.3 Seasonal and diurnal net CO₂ exchanges

20 Long-term data loss occurred in BB during the springs of 2011/2012, 2013/2014 and 2014/2015 and summers of 2013/2014 and 2014/2015, when annual C balances could not be estimated. However, by observing the available seasonal data, it is noticeable that, maximum and minimum seasonal net CO₂ exchanges were very different between sites (Fig. 4). On one hand, maximum seasonal net CO₂ uptake was measured during winter (December-February) in AMO and over spring (March-May) in BB, when peaking net CO₂ uptake fluxes equated to -31 g C m^{-2} (winter 2011/2012) and -105 g C m^{-2}
25 (spring 2010/2011) in AMO and BB, respectively. Additionally, net CO₂ uptake was only observed during three winters in the case of AMO, whereas it was frequently measured during both winter and spring in BB. On the other hand, cumulative net CO₂ release to the atmosphere occurred over all types of seasons in AMO, but acutely in summer, when maximum seasonal net CO₂ release was always observed ranging from 111 to 153 g C m^{-2} . In contrast, in BB, the highest CO₂ effluxes usually occurred in autumn ranging from 25 to 74 g C m^{-2} , although significant CO₂ release was also observed in winter
30 2013/2014 and the summers of 2009/2010-2011/2012.

Comparing daily-scale net CO₂ exchange and evapotranspiration (ET) fluxes with punctual Enhanced Vegetation Index (EVI) data, we can notice some similarities in the general patterns of both sites (Fig. 5). Roughly, there was a common



annual pattern at both sites in which the highest values of EVI coincided with maximum net CO₂ uptake rates (i.e. negative net CO₂ fluxes), which in turn, corresponded to peaking ET fluxes. Additionally, a decreasing trend in EVI over the 6 years of study was also noticeable for both sites. However, some inter-site and inter-annual differences were evident (Fig. 5).

On one hand, there were two main differences between sites. Firstly, extreme net CO₂ release was measured uniquely in AMO during summer months (June-August), when maximum net CO₂ fluxes ranging from 31 to 68 g C m⁻² were measured (Fig. 5b). Over the study period, the monthly net CO₂ exchange of AMO during dry seasons was up to one hundred times higher than in BB (in August 2013), since monthly net CO₂ fluxes measured in BB were much lower, from -8 to 16 g C m⁻² (Fig. 5b). Besides the striking differences in summer net CO₂ exchange between sites, minor discrepancies were also found in ET fluxes and EVI for the same drought periods. In this regard, monthly averaged ET over the dry season equated to 13 ± 4 and 10 ± 4 mm for AMO and BB, respectively, and EVI was on average 4% higher in BB than in AMO (Fig. 5a,c). The second inter-site difference was the greater net CO₂ uptake over longer periods measured in BB. Concretely, the period during which the ecosystems acted as C sinks lasted on average 38 days longer in BB than in AMO annually (Table 3). Accordingly, the annual amount of C fixation ranged from 6-59 g C m⁻² at AMO and 15-129 g C m⁻² at BB, respectively, with the annual averaged net C uptake in BB 162% higher than at AMO (Table 3). Consequently, peaking EVI values were usually observed during March-April for both sites, however, over winter and spring months (growing period), EVI measured at BB was 3 - 37% higher than AMO, with the largest inter-site differences in 2009/2010 and 2014/2015 (Fig. 5a). Likewise, monthly averaged ET fluxes measured at BB over winter and spring months (December-May) were from 3 to 24% larger than those measured at AMO. Additionally, the growing period of the driest year (2013/2014) corresponded to the lowest monthly ET fluxes and the least difference between sites.

On the other hand, differences in the inter-annual variability of EVI, carbon and water fluxes were also observed; however, due to long-term data losses at BB, accurate and comparative inter-annual analysis could not be done with carbon and water fluxes. In this sense, 2009/2010 and 2013/2014 were the years with maximum and minimum annual precipitation and EVI observations, respectively, for both sites. Concretely, in 2009/2010, EVI observations were 28% and 20% higher than the six-year averaged values in BB and AMO, respectively. In case of the driest year, 2013/2014, growing season (winter-spring) EVI was reduced 35% and 28% in BB and AMO, respectively. Nevertheless, the largest difference between sites in winter-spring EVI observations was found in 2014/2015, following the driest year, when BB showed a pattern very similar to those registered over the years previous to the dry spell, while AMO still presented EVI values 21% below the six-year average (Fig. 5a).

3.4 Differences in meteorological and soil variables between sites

Results from the two-sided Wilcoxon summed rank test (Table 4) showed significant differences (p-value < 0.05) between sites in most of the monitored meteorological variables. The few exceptions were the friction velocity (u_*), when using the whole study period, the maximum wind speed registered every half-hour (WS_{max}), when analyzing May-September data, and the wind speed (WS) and precipitation when assessing daytime May-September data (Table 4). The great amount of



observations (n ranged from 21410 to 205751) produced highly significant results (Table 4). Hence, the standardized difference between the samples (Diff_{st}) allowed us to quantitatively explore the differences between sites. Relevant differences ($\text{Diff}_{\text{st}} > 1$) were found only for pressure when using all databases, due to the distinct altitude of monitored sites.

Regarding soil variables, important differences ($\text{Diff}_{\text{st}} > 1$) between sites were detected in subsoil CO_2 molar fraction measured at 1.50 m depth ($\text{CO}_{2, 1.50\text{m}}$) for all periods, and during May-September months even when using only daytime data (Table 5). Concretely, $\text{CO}_{2, 1.50\text{m}}$ was always higher in AMO, from 889 to 1109 ppm (Table S1, S2 and S3). Additionally, volumetric water content at 0.05m depth ($\text{VWC}_{0.05\text{m}}$) was also higher in AMO compared to BB but only during summer months (Table 5), when absolute differences were very small, ranging from 0.028 to 0.037 $\text{m}^3 \text{m}^{-3}$ (Tables S1, S2 and S3). In contrast, subsoil CO_2 molar fraction measured at 0.05 m depth ($\text{CO}_{2, 0.05\text{m}}$) was from 89 to 150 ppm higher in BB when analyzing dry season (May-September) daytime data (Table 5, S1, S2 and S3).

The temporal dynamics of subsoil CO_2 molar fractions revealed similar annual patterns between sites; generally however, $\text{CO}_{2, 0.05\text{m}}$ was higher in BB, from 6 to 88%, while $\text{CO}_{2, 1.50\text{m}}$ was always greater in AMO, from 31 to 97% (Fig. 6). On one hand, the maximum monthly averaged values of $\text{CO}_{2, 0.05\text{m}}$ were registered in autumn, concretely, in November and October with 642 and 1120 ppm in AMO and BB, respectively, whereas minimum values occurred in September and August with 373 and 400 ppm at each site (Fig. 6a). On the other hand, peaking monthly averaged values of $\text{CO}_{2, 1.50\text{m}}$ occurred in July for both sites, with 2751 and 1602 ppm in AMO and BB, respectively, although relatively high $\text{CO}_{2, 1.50\text{m}}$ was also measured during November in BB. On the contrary, minimum values were observed in December and February, with 1364 and 735 ppm in AMO and BB, respectively (Fig. 6b).

Finally, results of the Spearman correlation analysis between pressure and belowground CO_2 at 1.50 m depth ($\text{CO}_{2, 1.50\text{m}}$) showed a negative relationship between both variables. Additionally, although most of the coefficients were significant (p -value < 0.05), higher correlations were found in AMO compared to BB (Table 6). Spearman correlation coefficients (r_s) were maxima at 12 h intervals for $\text{CO}_{2, 1.50\text{m}}$ and pressure increments ($dP_{12\text{h}}$) at AMO, and at 6 h intervals for $\text{CO}_{2, 1.50\text{m}}$ and pressure increments ($dP_{6\text{h}}$, respectively) at BB, with r_s equal to -0.87 and -0.63, respectively.

4 Discussion

Our results verify that land-degradation affects the C sequestration capacity of semiarid ecosystems, since relevant differences between sites were observed during the growing season, when greater net C uptake over longer periods was observed in the “natural” site (BB). However, contrary to what we previously hypothesized, much greater net C release was measured at the “degraded” site (AMO) over drought periods due to the predominance of subterranean ventilation (López-Ballesteros et al., 2017). In fact, the great difference in annual C budgets between sites (Fig. 2) was largely related to this process resulting in an average release of 196 ± 40 and $-23 \pm 20 \text{ g C m}^{-2} \text{ yr}^{-1}$ for the “degraded” (AMO) and “natural” (BB) sites, respectively. In this regard, the ecosystems’ functioning could be divided into three different phases. The first phase corresponded to the autumn months, when the first rainfall events after the dry summer (i.e. rain pulses) activated the soil



microbiota triggering respiratory CO₂ emissions as previously measured at the same experimental sites (López-Ballesteros et al., 2016; Rey et al., 2017). During this phase, maximum CO₂ release was observed at BB, however higher CO₂ release was usually measured at AMO (Fig. 4), maybe due to the greater hydric stress experienced prior to rewetting, the differences in microbial communities (Rey et al., 2017), and the greater pool of soil inorganic carbon (Emmerich, 2003; Table 1). The second phase comprised the growing period, when plants photosynthesized and also respired along with microorganisms under milder temperatures and better hydric conditions. During this phase, larger net CO₂ uptake was measured in BB, concretely 162% more than in AMO (Table 3) due to the higher vegetation cover and more fertile soils (Table 1) of the “natural” site. Moreover, this result was supported by the lower ET and EVI values obtained in AMO during winter and spring months of the whole study period (Fig. 5). The third phase consisted of the dormancy period when water scarcity and high temperatures constrained biological activity. During this period, as stated previously, a neutral C balance was observed in BB while extreme CO₂ release was measured in AMO.

In order to detect potential factors driving the observed differences in the C balances, we checked whether soil and meteorological variables differed between sites. Our results demonstrated that some factors typically influencing gross primary production (GPP) and ecosystem respiration (R_{eco}), and hence net ecosystem CO₂ exchange, such as photosynthetic photon flux density (PPFD; Michaelis and Menten, 1913), precipitation (Berner et al., 2017; Jongen et al., 2011), vapor pressure deficit (VPD; Lasslop et al., 2010) and soil and air temperature (Lloyd and Taylor, 1994), did not differ between sites (Table 4, 5). Conversely, some differences were found for shallow soil volumetric water content (VWC_{0.05m}) during dry seasons (Table 5), when VWC_{0.05m} was two times higher in AMO than in BB, but absolute differences were slight, from 0.028 to 0.037 m³ m⁻³ (Tables S1, S2 and S3). Hence, although the important influence of soil moisture in both GPP and R_{eco} is known (Tang and Baldocchi, 2005), we believe that differences in VWC_{0.05m} are not relevant enough to cause the differing ecosystems’ functioning observed over the drought period. Additionally, we think that this inter-site difference in VWC_{0.05m} could be instrumental, or due to the spatial variability of VWC_{0.05m} derived from the heterogeneity of soil morphological characteristics, since we only used one sensor at each site.

Similarly, important differences were not detected in several variables linked to subterranean ventilation, such as the friction velocity (u*; Kowalski et al., 2008), wind speed (WS; Rey et al., 2012), half-hourly maximum wind speed (WS_{max}) and net radiation, which has been positively correlated to ventilative CO₂ fluxes (López-Ballesteros et al., 2017), when using the analysis periods when this process is supposed to be relevant, namely daytime hours during the dry seasons (Table 4). In contrast, inter-site differences were found in net radiation (Table 4). However, although no turbulence and wind speed inter-site differences were found, interconnectivity of soil pores and fractures is probably higher at AMO (Table 1) due to its higher gravel and rock fractions (Table 1), which could lead to an enhanced penetration of eddies within the vadose zone (Pérez-Priego et al., 2013).

Apart from that, outstanding differences between sites were observed in subsoil CO₂ molar fractions measured at 0.05 and 1.50 m depths (CO_{2,0.05m} and CO_{2,1.50m}, respectively; Table 5). On one hand, CO_{2,0.05m} was generally higher in BB given its



lower degradation level, which probably promotes a higher microbial activity supported by higher vegetation density and soil fertility (Table 1) especially during spring (Fig. 6), as pointed also by Oyonarte et al. (2012). On the other hand, CO_2 ,_{1.50m} values were acutely higher in AMO, by up to 1000 ppm compared to BB (Tables S1, S2 and S3). Therefore, we suggest that CO_2 ,_{1.50m} is the main factor responsible for the inter-site differences in net CO_2 fluxes over the dry season. However, not only the amount of subsoil CO_2 matters but also how effective is its transport, since both determine the net CO_2 release from the vadose zone to the atmosphere. In this context, Oyonarte et al. (2012) found, in the same study area (Cabo de Gata-Níjar Natural Park), that soils with degradation symptoms, such as lower SOC, depleted biological activity, coarser texture and worse structure, showed higher soil CO_2 effluxes over the dry season. Additionally, soil CO_2 effluxes measured during summer months correlated positively with the fraction of rock outcrops, suggesting that deteriorated soil physical conditions actually enhanced vertical transfer of CO_2 -rich air from subsoil to the atmosphere (Oyonarte et al., 2012). In fact, correlation analysis between CO_2 ,_{1.50m} and atmospheric pressure (Table 6) showed a stronger relationship between both variables at AMO. In this sense, ecosystem degradation could provoke a greater exposure of subsoil CO_2 to the pressure effect, as described by Sánchez-Cañete et al. (2013), probably due to a higher fraction of bare soil, coarser structure, differing porosity type and/or thinner soil depth (Table 1).

Regarding EVI data, these results have allowed us to complement our findings based on CO_2 fluxes, especially when EC data losses occurred. For instance, the declining trend observed from 2009/2010 until the end of the study period, for both sites, was not noticeable from EC data alone (Fig. 5). This long-term decrease in EVI may be related to a gradual drying following the wettest year (2009/2010), when extraordinarily high precipitation (twice the annual average precipitation for both sites over the study period) occurred. This EVI pattern also denotes a pulse-like behaviour of ecosystem vegetation over the inter-annual time scale. Moreover, in addition to demonstrating that degradation can influence the biological activity of ecosystems' vegetation, EVI results also showed that degradation level can modulate how an ecosystem responds to a short-term change. A clear example is the dry spell experienced in 2013/2014, when a reduction in EVI was measured during the growing season in both sites, i.e. 35% and 28% in BB and AMO, respectively. However, a year later (2014/2015), EVI values below the six-year average were observed only at AMO (21% lower; Fig. 5a). Accordingly, the “natural” site (BB) seemed to be more stable than the “degraded” site (AMO) against the short-term disturbance, since the effect of drought persisted in AMO even during the following year, while BB recovered to a pre-perturbation state within the same period (Fig. 5a). As a result, ecosystem resilience, defined by Holling (1973) as the amount of disturbance that a system can withstand without changing state, was lessened by long-term disturbances such as degradation, making degraded ecosystems more vulnerable to climate extremes (Reichstein et al., 2013). In this sense, mitigation policies to confront land degradation should be focused on prevention programs since ecosystem restoration does not recover complete ecosystem functionality (Lal, 2001; Moreno-Mateos et al., 2017). Moreover, even after several decades, relict degradation legacies can remain (Alados et al., 2011).



5 Conclusions

The present study can be seen as a step forward to better understanding the effect of land degradation on the intricate network of multi-scale processes, factors and structures that define ecosystems' biological productivity and ultimately control their C balances. Despite some limitations, such as long-term data gaps, this research demonstrates that continuous ecosystem-scale EC observations remain crucial to comprehend how climate and land use change can modify the C sequestration capacity of ecosystems. In fact, annual average release of 196 ± 40 and -23 ± 20 g C m⁻² yr⁻¹ for the “degraded” and “natural” (i.e. site of reference) sites were measured, respectively. Additionally, larger net CO₂ uptake over longer periods was observed at the “natural” site, concretely an amount of C 162% higher compared to the “degraded” site, whereas much greater net CO₂ release was measured at the “degraded” site during drought periods. Future research should be based on the continuity of long-term monitoring stations, such as eddy covariance stations, in order to calibrate and validate satellite data, reduce uncertainties in the relationships between ecosystem productivity, land degradation and climate change and finally, to improve the predictive ability of current terrestrial C models.

Data availability

The eddy covariance data are available in the European Database Cluster (<http://www.europe-fluxdata.eu>) where experimental sites have the codes “Es-Amo” and “Es-Agu”. Other data can be obtained by contacting the corresponding author.

Author contribution

FD, CO, AK and PSO designed the experiment. ALB, PSO, EPSC and MRM calibrated the sensors, collected the data and maintained the field instrumentation. EPSC designed subsoil data acquisition system and MRM processed subsoil data. ALB processed the eddy covariance data, made the figures and tables and wrote the manuscript. All authors reviewed the manuscript.

Acknowledgements

A. López-Ballesteros acknowledges support from the Spanish Ministry of Economy and Competitiveness (FPI grant, BES-2012-054835). This work was supported in part by the Spanish Ministry of Economy and Competitiveness projects ICOS-SPAIN (AIC10-A-000474), SOILPROF (CGL2011-15276-E), GEI-Spain (CGL2014-52838-C2-1-R), including European Union ERDF funds; and by the European Commission project DIESEL (PEOPLE-2013-IOF-625988). We also thank L. Morillas, O. Uclés and E. Arnau for field work.



References

- Ahlström, A., Raupach, M. R., Schurgers, G., Smith, B., Arneeth, A., Jung, M., Reichstein, M., Canadell, J. G., Friedlingstein, P., Jain, A. K., Kato, E., Poulter, B., Sitch, S., Stocker, B. D., Viovy, N., Wang, Y. P., Wiltshire, A., Zaehle, S., and Zeng, N.: The dominant role of semi-arid ecosystems in the trend and variability of the land CO₂ sink, *Science*, 348, 895-899, 10.1126/science.aaa1668, 2015.
- Alados, C., Pueyo, Y., Barrantes, O., Escós, J., Giner, L., and Robles, A.: Variations in landscape patterns and vegetation cover between 1957 and 1994 in a semiarid Mediterranean ecosystem, *Landscape ecology*, 19, 543-559, 2004.
- Alados, C. L., Puigdefábregas, J., and Martínez-Fernández, J.: Ecological and socio-economical thresholds of land and plant-community degradation in semi-arid Mediterranean areas of southeastern Spain, *Journal of Arid Environments*, 75, 1368-1376, 2011.
- Bajocco, S., De Angelis, A., and Salvati, L.: A satellite-based green index as a proxy for vegetation cover quality in a Mediterranean region, *Ecological Indicators*, 23, 578-587, 2012.
- Baldocchi, D. D., Hincks, B. B., and Meyers, T. P.: Measuring biosphere-atmosphere exchanges of biologically related gases with micrometeorological methods, *Ecology*, 69, 1331-1340, 1988.
- Berner, L. T., Law, B. E., and Hudiburg, T. W.: Water availability limits tree productivity, carbon stocks, and carbon residence time in mature forests across the western US, *Biogeosciences*, 14, 365-378, 2017.
- Bown, H. E., Fuentes, J.-P., Perez-Quezada, J. F., and Franck, N.: Soil respiration across a disturbance gradient in sclerophyllous ecosystems in Central Chile, *Ciencia e Investigación Agraria*, 41, 89-106, 2014.
- Cook, B. I., Smerdon, J. E., Seager, R., and Coats, S.: Global warming and 21st century drying, *Climate Dynamics*, 43, 2607-2627, 10.1007/s00382-014-2075-y, 2014.
- del Barrio, G., Puigdefábregas, J., Sanjuan, M. E., Stellmes, M., and Ruiz, A.: Assessment and monitoring of land condition in the Iberian Peninsula, 1989–2000, *Remote Sensing of Environment*, 114, 1817-1832, <http://dx.doi.org/10.1016/j.rse.2010.03.009>, 2010.
- Emmerich, W. E.: Carbon dioxide fluxes in a semiarid environment with high carbonate soils, *Agricultural and Forest Meteorology*, 116, 91-102, 10.1016/s0168-1923(02)00231-9, 2003.
- Feng, Q., Liu, W., Yanwu, Z., Jianhua, S., Yonghong, S., Zun Qiang, C., and Haiyang, X.: Effect of climatic changes and human activity on soil carbon in desertified regions of China, *Tellus B*, 58, 117-128, 2006.
- Feng, S., and Fu, Q.: Expansion of global drylands under a warming climate, *Atmos. Chem. Phys.*, 13, 10081-10094, 10.5194/acp-13-10081-2013, 2013.
- Fensholt, R., Rasmussen, K., Kaspersen, P., Huber, S., Horion, S., and Swinnen, E.: Assessing land degradation/recovery in the African Sahel from long-term earth observation based primary productivity and precipitation relationships, *Remote Sensing*, 5, 664-686, 2013.



- Gao, X., and Giorgi, F.: Increased aridity in the Mediterranean region under greenhouse gas forcing estimated from high resolution simulations with a regional climate model, *Global and Planetary Change*, 62, 195-209, 10.1016/j.gloplacha.2008.02.002, 2008.
- Holling, C. S.: Resilience and Stability of Ecological Systems, *Annual Review of Ecology and Systematics*, 4, 1-23, 1973.
- 5 Hou, X., Wang, Z., Michael, S. P., Ji, L., and Yun, X.: The response of grassland productivity, soil carbon content and soil respiration rates to different grazing regimes in a desert steppe in northern China, *The Rangeland Journal*, 36, 573-582, 2014.
- Jongen, M., Pereira, J. S., Aires, L. M. I., and Pio, C. A.: The effects of drought and timing of precipitation on the inter-annual variation in ecosystem-atmosphere exchange in a Mediterranean grassland, *Agricultural and Forest Meteorology*, 151, 595-606, 2011.
- 10 Kowalski, A. S., Serrano-Ortiz, P., Janssens, I. A., Sánchez-Moral, S., Cuezva, S., Domingo, F., Were, A., and Alados-Arboledas, L.: Can flux tower research neglect geochemical CO₂ exchange?, *Agricultural and Forest Meteorology*, 148, 1045-1054, 2008.
- Kottek, M., Grieser, J., Beck, C., Rudolf, B., and Rubel, F.: World map of the Köppen-Geiger climate classification updated, *Meteorologische Zeitschrift*, 15, 259-263, 2006.
- 15 Lal, R.: Potential of Desertification Control to Sequester Carbon and Mitigate the Greenhouse Effect, *Climatic Change*, 51, 35-72, 10.1023/a:1017529816140, 2001.
- Lasslop, G., Reichstein, M., Papale, D., Richardson, A. D., Arneeth, A., Barr, A., Stoy, P., and Wohlfahrt, G.: Separation of net ecosystem exchange into assimilation and respiration using a light response curve approach: critical issues and global evaluation, *Global Change Biology*, 16, 187-208, 10.1111/j.1365-2486.2009.02041.x, 2010.
- 20 Leon, E., Vargas, R., Bullock, S., Lopez, E., Panosso, A. R., and La Scala Jr, N.: Hot spots, hot moments, and spatio-temporal controls on soil CO₂ efflux in a water-limited ecosystem, *Soil Biology and Biochemistry*, 77, 12-21, <http://dx.doi.org/10.1016/j.soilbio.2014.05.029>, 2014.
- Lloyd, J., and Taylor, J.: On the temperature dependence of soil respiration, *Functional ecology*, 315-323, 1994.
- López-Ballesteros, A., Serrano-Ortiz, P., Sánchez-Cañete, E. P., Oyonarte, C., Kowalski, A. S., Pérez-Priego, Ó., and Domingo, F.: Enhancement of the net CO₂ release of a semiarid grassland in SE Spain by rain pulses, *Journal of Geophysical Research: Biogeosciences*, 121, 2015JG003091, 10.1002/2015jg003091, 2016.
- López-Ballesteros, A., Serrano-Ortiz, P., Kowalski, A. S., Sánchez-Cañete, E. P., Scott, R. L., and Domingo, F.: Subterranean ventilation of allochthonous CO₂ governs net CO₂ exchange in a semiarid Mediterranean grassland, *Agricultural and Forest Meteorology*, 234–235, 115-126, <http://dx.doi.org/10.1016/j.agrformet.2016.12.021>, 2017.
- 30 Ma, S., Baldocchi, D., Wolf, S., and Verfaillie, J.: Slow ecosystem responses conditionally regulate annual carbon balance over 15 years in Californian oak-grass savanna, *Agricultural and Forest Meteorology*, 228–229, 252-264, <http://dx.doi.org/10.1016/j.agrformet.2016.07.016>, 2016.
- Mainguet, M., and Da Silva, G.: Desertification and drylands development: what can be done?, *Land Degradation & Development*, 9, 375-382, 1998.



- Mauder, M., Foken, T.: Documentation and instruction manual of the eddy covariance software package324 TK3. *AbtMikrometeorologie* 46, 60, 2004.
- Mbow, C., Brandt, M., Ouedraogo, I., de Leeuw, J., and Marshall, M.: What four decades of earth observation tell us about land degradation in the Sahel?, *Remote Sensing*, 7, 4048-4067, 2015.
- 5 Michaelis, L., Menten, M.L.: Die Kinetik der Invertinwirkung. *Biochem. Z.* 49, 333–369. 1913.
- Moncrieff, J. B., Massheder, J. M., de Bruin, H., Elbers, J., Friborg, T., Heusinkveld, B., Kabat, P., Scott, S., Soegaard, H., and Verhoef, A.: A system to measure surface fluxes of momentum, sensible heat, water vapour and carbon dioxide, *Journal of Hydrology*, 188–189, 589-611, [http://dx.doi.org/10.1016/S0022-1694\(96\)03194-0](http://dx.doi.org/10.1016/S0022-1694(96)03194-0), 1997.
- Moreno-Mateos, D., Barbier, E. B., Jones, P. C., Jones, H. P., Aronson, J., López-López, J. A., McCrackin, M. L., Meli, P.,
10 Montoya, D., and Rey Benayas, J. M.: Anthropogenic ecosystem disturbance and the recovery debt, *Nature Communications*, 8, 14163, 10.1038/ncomms14163
- Niemeijer, D., Puigdefabregas, J., White, R., Lal, R., Winslow, M., Ziedler, J., Prince, S., Archer, E., King, C.: *Dryland Systems*, in: *Ecosystems and Human Well-being: Current State and Trends, Volume 1, Millennium Ecosystem Assessment Series*, Island Press, Washington, USA, 625, 2005.
- 15 Omuto, C., Vargas, R., Alim, M., and Paron, P.: Mixed-effects modelling of time series NDVI-rainfall relationship for detecting human-induced loss of vegetation cover in drylands, *Journal of Arid Environments*, 74, 1552-1563, 2010.
- Omuto, C.: A new approach for using time-series remote-sensing images to detect changes in vegetation cover and composition in drylands: A case study of eastern Kenya, *International journal of remote sensing*, 32, 6025-6045, 2011.
- Oñate Rubalcaba, J.J.: *Caracterización de los cambios climáticos en la península ibérica y Canarias desde principios de siglo*.
20 Thesis Report. Autónoma de Madrid. 1993.
- Oyonarte, C., Rey, A., Raimundo, J., Miralles, I., and Escribano, P.: The use of soil respiration as an ecological indicator in arid ecosystems of the SE of Spain: Spatial variability and controlling factors, *Ecological Indicators*, 14, 40-49, <http://dx.doi.org/10.1016/j.ecolind.2011.08.013>, 2012.
- Pérez-Priego, O., Serrano-Ortiz, P., Sánchez-Cañete, E. P., Domingo, F., and Kowalski, A. S.: Isolating the effect of
25 subterranean ventilation on CO₂ emissions from drylands to the atmosphere, *Agricultural and Forest Meteorology*, 180, 194-202, 2013.
- Poulter, B., Frank, D., Ciais, P., Myneni, R. B., Andela, N., Bi, J., Broquet, G., Canadell, J. G., Chevallier, F., Liu, Y. Y., Running, S. W., Sitch, S., and Van Der Werf, G. R.: Contribution of semi-arid ecosystems to interannual variability of the global carbon cycle, *Nature*, 509, 600-603, 10.1038/nature13376, 2014.
- 30 Prince, S., Becker-Reshef, I., and Rishmawi, K.: Detection and mapping of long-term land degradation using local net production scaling: Application to Zimbabwe, *Remote Sensing of Environment*, 113, 1046-1057, 2009.
- Puigdefábregas, J., and Mendizabal, T.: Perspectives on desertification: western Mediterranean, *Journal of Arid Environments*, 39, 209-224, 1998.



- Reichstein, M., Falge, E., Baldocchi, D., Papale, D., Aubinet, M., Berbigier, P., Bernhofer, C., Buchmann, N., Gilmanov, T., Granier, A., Grünwald, T., Havránková, K., Ilvesniemi, H., Janous, D., Knohl, A., Laurila, T., Lohila, A., Loustau, D., Matteucci, G., Meyers, T., Miglietta, F., Ourcival, J.-M., Pumpanen, J., Rambal, S., Rotenberg, E., Sanz, M., Tenhunen, J., Seufert, G., Vaccari, F., Vesala, T., Yakir, D., and Valentini, R.: On the separation of net ecosystem exchange into
5 assimilation and ecosystem respiration: review and improved algorithm, *Global Change Biology*, 11, 1424-1439, 10.1111/j.1365-2486.2005.001002.x, 2005.
- Reichstein, M., Bahn, M., Ciais, P., Frank, D., Mahecha, M. D., Seneviratne, S. I., Zscheischler, J., Beer, C., Buchmann, N., Frank, D. C., Papale, D., Rammig, A., Smith, P., Thonicke, K., Van Der Velde, M., Vicca, S., Walz, A., and Wattenbach, M.: Climate extremes and the carbon cycle, *Nature*, 500, 287-295, 10.1038/nature12350, 2013.
- 10 Rey, A., Pegoraro, E., Oyonarte, C., Were, A., Escribano, P., and Raimundo, J.: Impact of land degradation on soil respiration in a steppe (*Stipa tenacissima* L.) semi-arid ecosystem in the SE of Spain, *Soil Biology and Biochemistry*, 43, 393-403, 2011.
- Rey, A., Belelli-Marchesini, L., Were, A., Serrano-ortiz, P., Etiope, G., Papale, D., Domingo, F., and Pegoraro, E.: Wind as a main driver of the net ecosystem carbon balance of a semiarid Mediterranean steppe in the South East of Spain, *Global
15 Change Biology*, 18, 539-554, 10.1111/j.1365-2486.2011.02534.x, 2012.
- Rey, A., Oyonarte, C., Morán-López, T., Raimundo, J., and Pegoraro, E.: Changes in soil moisture predict soil carbon losses upon rewetting in a perennial semiarid steppe in SE Spain, *Geoderma*, 287, 135-146, <http://dx.doi.org/10.1016/j.geoderma.2016.06.025>, 2017.
- Rodríguez-Fernández, L. R., López-Olmedo, F., Oliveira, J. T., Medialdea, T., Terrinha, P., Matas, J., Martín-Serrano, A.,
20 Martín-Parra, L. M., Rubio, F., Marín, C., Montes, M. and Nozal, F.: Mapa geológico de la Península Ibérica, Baleares y Canarias a escala 1/1.000.000. Instituto Geológico y Minero de España (IGME). 2015.
- Sánchez-Cañete, E. P., Kowalski, A. S., Serrano-Ortiz, P., Pérez-Priego, O., and Domingo, F.: Deep CO₂ soil inhalation/exhalation induced by synoptic pressure changes and atmospheric tides in a carbonated semiarid steppe, *Biogeosciences*, 10, 6591-6600, 2013.
- 25 Schulz, K., Voigt, K., Beusch, C., Almeida-Cortez, J. S., Kowarik, I., Walz, A., and Cierjacks, A.: Grazing deteriorates the soil carbon stocks of Caatinga forest ecosystems in Brazil, *Forest Ecology and Management*, 367, 62-70, 2016.
- Serrano-Ortiz, P., Domingo, F., Cazorla, A., Were, A., Cuezva, S., Villagarcía, L., Alados-Arboledas, L., and Kowalski, A. S.: Interannual CO₂ exchange of a sparse Mediterranean shrubland on a carbonaceous substrate, *Journal of Geophysical Research G: Biogeosciences*, 114, 2009.
- 30 Serrano-Ortiz, P., Oyonarte, C., Pérez-Priego, O., Reverter, B., Sánchez-Cañete, E. P., Were, A., Uclés, O., Morillas, L., and Domingo, F.: Ecological functioning in grass-shrub Mediterranean ecosystems measured by eddy covariance, *Oecologia*, 175, 1005-1017, 10.1007/s00442-014-2948-0, 2014.
- Shoshany, M., and Karnibad, L.: Remote Sensing of Shrubland Drying in the South-East Mediterranean, 1995–2010: Water-Use-Efficiency-Based Mapping of Biomass Change, *Remote Sensing*, 7, 2283-2301, 2015.



Tang, J., and Baldocchi, D. D.: Spatial–temporal variation in soil respiration in an oak–grass savanna ecosystem in California and its partitioning into autotrophic and heterotrophic components, *Biogeochemistry*, 73, 183-207, 2005.

Thompson, M., Vlok, J., Rouget, M., Hoffman, M., Balmford, A., and Cowling, R.: Mapping grazing-induced degradation in a semi-arid environment: a rapid and cost effective approach for assessment and monitoring, *Environmental management*, 5 43, 585, 2009.

Uclés, O., Villagarcía, L., Moro, M. J., Canton, Y., and Domingo, F.: Role of dewfall in the water balance of a semiarid coastal steppe ecosystem, *Hydrological Processes*, 28, 2271-2280, 10.1002/hyp.9780, 2014.

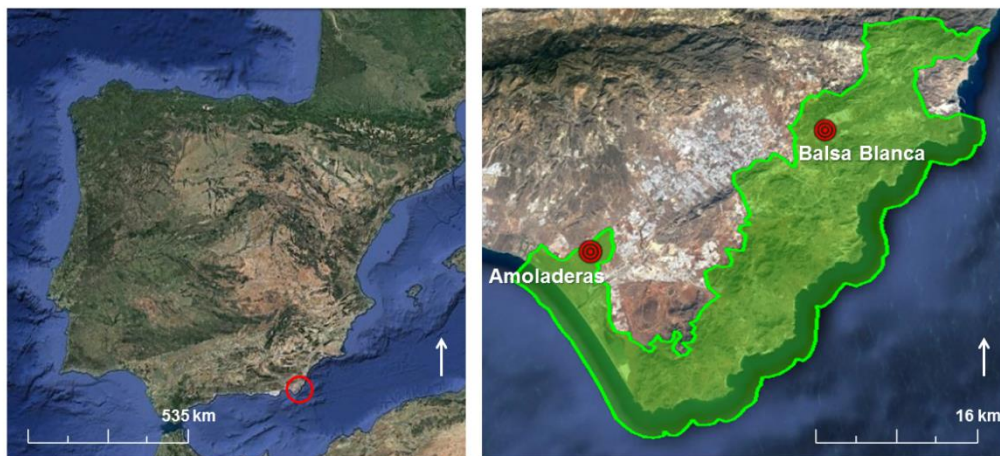
United Nations Convention to Combat Desertification (UNCCD): General Assembly. 1994.

Wang, W., Guo, J., and Oikawa, T.: Contribution of root to soil respiration and carbon balance in disturbed and undisturbed 10 grassland communities, northeast China, *Journal of Biosciences*, 32, 375-384, 2007.

Wang, Y., Yan, X., and Wang, Z.: A preliminary study to investigate the biogeophysical impact of desertification on climate based on different latitudinal bands, *International Journal of Climatology*, 36, 945-955, 10.1002/joc.4396, 2016.

Watanabe, M. D. B., and Ortega, E.: Ecosystem services and biogeochemical cycles on a global scale: valuation of water, carbon and nitrogen processes, *Environmental Science & Policy*, 14, 594-604, 15 <http://dx.doi.org/10.1016/j.envsci.2011.05.013>, 2011.

Zika, M., and Erb, K.-H.: The global loss of net primary production resulting from human-induced soil degradation in drylands, *Ecological Economics*, 69, 310-318, 2009.



5 **Figure 1: Location of the experimental sites. Green area represents the Cabo de Gata-Níjar Natural Park (Almeria, Spain).**



Table 1: Site characteristics, surface fractions and soil properties of both experimental sites studied. Asterisks denote significant differences (p -value<0.05). Adapted from Rey et al., (2011).

	Amoladeras	Balsa Blanca
<i>Site characteristics</i>		
Location	Almeria N36°50'5'' W2°15'1''	Almeria N36°56' 0'' W2°1'58''
Altitude (m)	65	208
Climate	Subtropical, dry, semiarid	Subtropical, dry, semiarid
Annual T	18	18
Annual P	220	220
Predominant sp.	<i>Machrocloa tenacissima</i>	<i>Machrocloa tenacissima</i>
<i>Surface fractions</i>		
Vegetation cover (%)	23.1 ± 2.4*	63.2 ± 5.2*
Litter (%)	10.5 ± 2.0	8.1 ± 1.9
Biological crust (%)	23.1 ± 2.8	18.2 ± 3.8
Bare soil (%)	8.1 ± 0.1*	0.3 ± 0.3*
Gravel (%)	21.1 ± 0.1*	8.6 ± 2.5*
Rock (%)	14.0 ± 1.2*	1.5 ± 0.5*
<i>Soil properties</i>		
Soil type	Lithic Leptosol (Calcaric)	Mollic Lithic Leptosol (Calcaric)
Maximum soil depth (cm)	10	20
Soil texture class	Sandy loam	Sandy loam
Clay (%)	14.6	16.1
Silt (%)	27.0	22.8
Sand (%)	58.4	61.1
Bulk density (g cm ⁻³)	1.11 ± 0.04	1.25 ± 0.09
SOC (kg m ⁻²)	1.24	4.64
Carbonates (%)	14	2


Table 2: Variables measured, sensors used and their installation height in Amoladeras and Balsa Blanca experimental sites.

Variable	Sensor	Sensors height	
		Amoladeras	Balsa Blanca
<i>Eddy Covariance system</i>			
Wind speed (3-D) and sonic temperature	A three-axis sonic anemometer (CSAT-3, Campbell Scientific Inc, Logan, UT, USA; hereafter CSI)	3.05 m	2.90 m
CO ₂ and H ₂ O vapour densities	A open-path infrared gas analyzer (Li- 7500, Li-Cor, Lincoln, NE, USA)	3.05 m	2.90 m
<i>Meteorological and soil measurements</i>			
Air pressure	A open-path infrared gas analyzer (Li-Cor 7500, Lincoln, NE, USA)	1.60 m	1.80 m
Photosynthetic Photon Flux Density	Two PAR sensors (Li-190, Li-Cor, Lincoln, NE, USA)	1.40 m	1.50 m
Net Radiation	A net radiometer (NR Lite, Kipp&Zonen, Delft, Netherlands)	1.70 m	1.50 m
Air temperature	A thermohygrometer (HMP35-C, CSI)	3.62 m	1.50 m
Air relative humidity	A thermohygrometer (HMP35-C, CSI)	3.62 m	1.50 m
Subsoil Water Content	Two water content reflectometers (CS616, CSI)	-0.05 and -1.50 m	-0.05 and -1.50 m
Subsoil temperature	Two soil temperature probes (TCAV, CSI)	-0.05 and -1.50 m	-0.05 and -1.50 m
Subsoil CO ₂ molar fraction	A CO ₂ sensor (GMP-343, Vaisala, Inc., Finland)	-0.05 m	-0.05 m
Subsoil CO ₂ molar fraction	A CO ₂ sensor (GMM222, Vaisala, Inc., Finland)	-1.50 m	-1.50 m
Rainfall	A tipping bucket (0.2 mm) rain gauge (785 M, Davis Instruments Corp., Hayward, CA, USA)	1.30 m	1.40 m

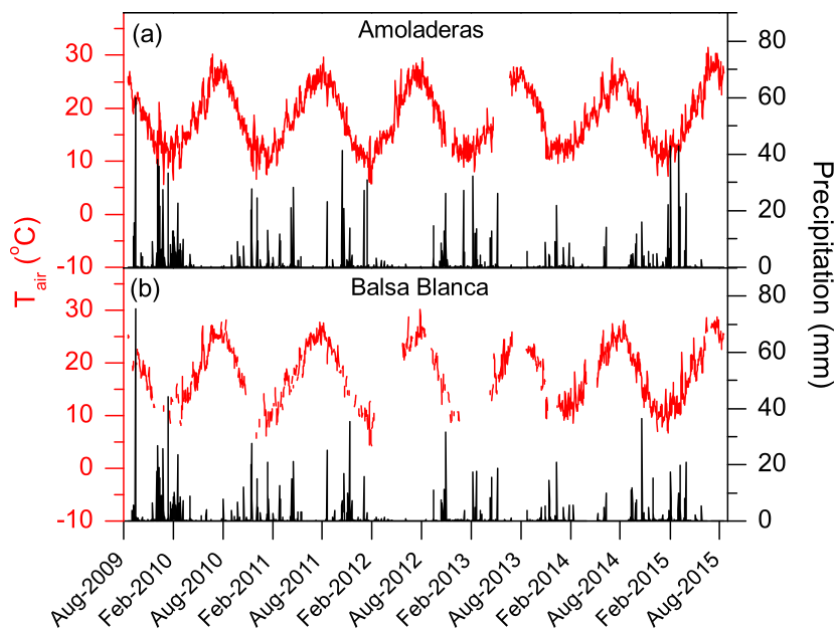
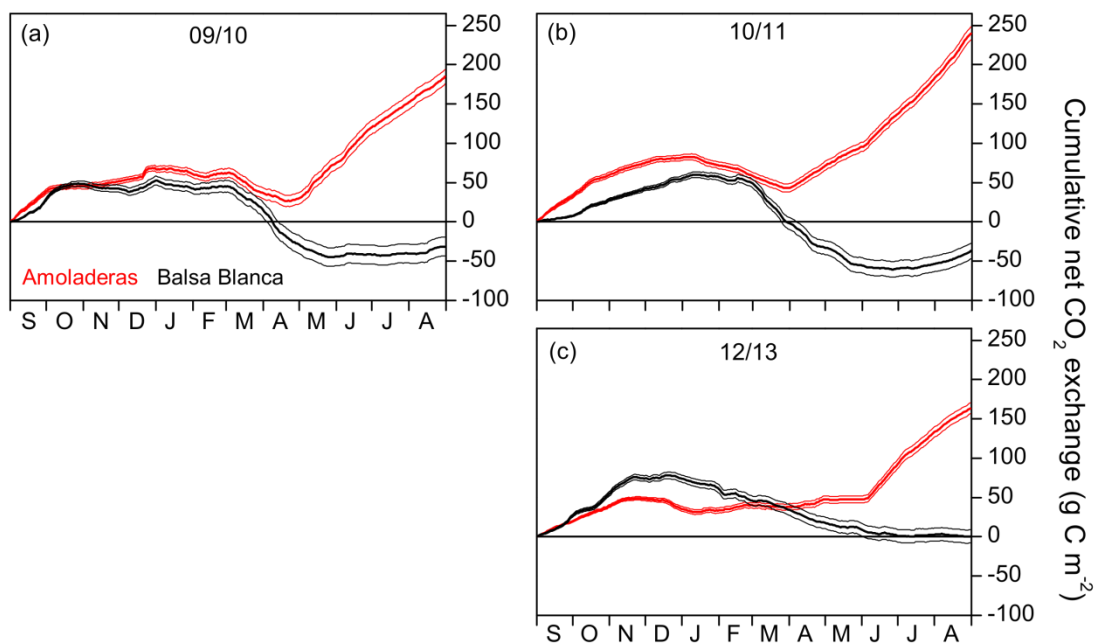


Figure 2: Daily averages of air temperature (T_{air}) and precipitation in (a) Amoladeras and (b) Balsa Blanca.



5

Figure 3: Cumulative annual net CO_2 exchange over the three hydrological years without long-periods of missing data in both experimental sites, Amoladeras (red lines) and Balsa Blanca (black lines). Negative values denote net carbon uptake while positive values denote net carbon release. Thin lines indicate uncertainty derived from the gap-filling procedure.

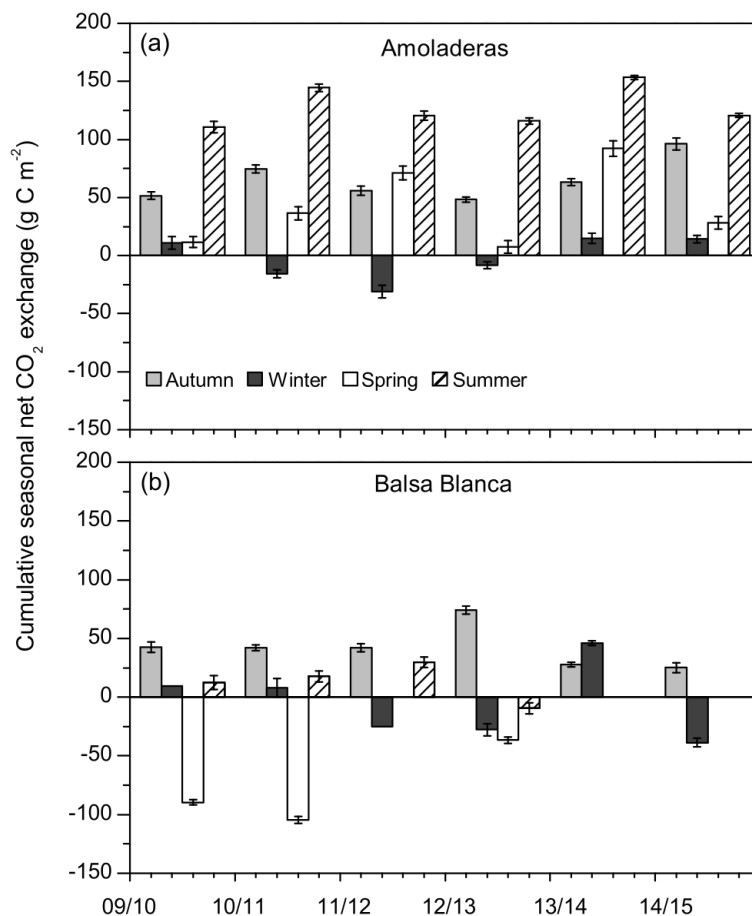
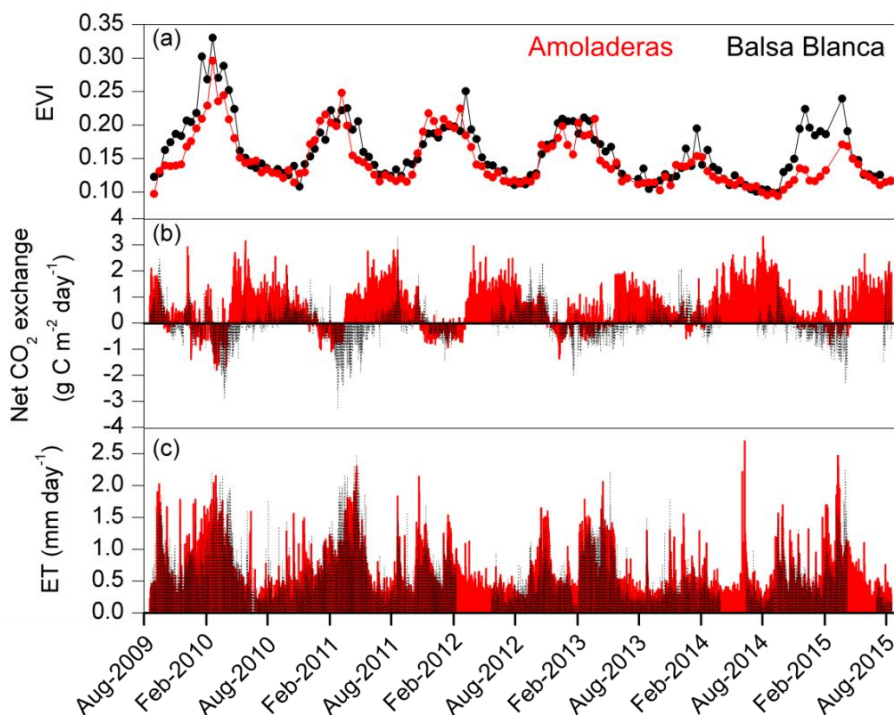


Figure 4: Cumulative seasonal net CO₂ exchange over the study period in both experimental sites. Negative values denote net carbon uptake while positive values denote net carbon release. In case of Balsa Blanca, lacking bars correspond to long-term data losses (>50% data).

5



5 **Figure 5: Time series of (a) Enhanced Vegetation Index (EVI), (b) daily net CO₂ exchange and (c) daily evapotranspiration fluxes measured in Amoladeras (red lines and dots) and Balsa Blanca (black lines and dots) over six hydrological years (2009-2015). Long-term data losses correspond to periods of several months when ET and CO₂ fluxes are absent.**

10 **Table 3: Number of days with daily net CO₂ uptake and the related total C absorbed for every hydrological year and every field site of the study. Asterisks denote those years with abundant data losses (~30% data).**

Site	Amoladeras		Balsa Blanca		
	Year	N. days of net CO ₂ uptake	Total net CO ₂ uptake (g C m ⁻²)	N. days of net CO ₂ uptake	Total net CO ₂ uptake (g C m ⁻²)
	09/10	58	-59 ± 7	196	-125 ± 12
	10/11	86	-41 ± 4	160	-129 ± 10
	11/12	114	-43 ± 5	104*	-40 ± 6*
	12/13	103	-31 ± 4	212	-96 ± 8
	13/14	31	-6 ± 12	64*	-15 ± 5*
	14/15	59	- 14 ± 3	172*	-103 ± 9*



5 **Table 4: Results of the two-sided Wilcoxon summed rank test used to assess differences among meteorological variables measured at each experimental site over all periods, from May to September and from May to September during daytime, separately. Medians of the difference between the samples (Amoladeras minus Balsa Blanca) in standardized terms (Diff_{st}) and number of observations are detailed. Significant results ($p\text{-value} < 0.05$) are denoted with asterisks, and bold values represent those variables with Diff_{st} between sites above 1.**

Variables	All periods		May - September		May - September Daytime	
	Diff_{st}	n	Diff_{st}	n	Diff_{st}	n
PPFD ($\mu\text{mol m}^{-2} \text{s}^{-1}$)	0.0009*	205751	0.0009*	84491	0.1378*	38963
Net radiation (W m^{-2})	-0.0457*	197924	-0.0476*	81019	-0.1205*	38963
T_{air} ($^{\circ}\text{C}$)	0.0310*	182240	0.1935*	77866	0.0502*	37480
VPD (hPa)	0.0783*	166918	0.1370*	71474	-0.0938*	34430
RH (%)	-0.1636*	197649	-0.1031*	80950	0.1784*	38935
u_* (m s^{-1})	-0.0054	166346	-0.0563*	71194	-0.1340*	34284
WS (m s^{-1})	0.1628*	166359	0.0793*	71195	0.0165	34285
WS_{max} (m s^{-1})	0.1001*	165458	0.0124	70635	-0.0796*	33994
Pressure (hPa)	1.6999*	166359	1.8696*	71195	1.8633*	34285
Precipitation (mm)	-1.95E-05*	204892	-4.84E-05*	83860	5.32E-05	38963

30 **Table 5: Results of the two-sided Wilcoxon summed rank test used to assess differences among soil variables measured at each experimental site over over all periods, from May to September and from May to September during daytime, separately. Medians of the difference between the samples (Amoladeras minus Balsa Blanca) in standardized terms (Diff_{st}) and number of observations are detailed. Significant results ($p\text{-value} < 0.05$) are denoted with asterisks, and bold values represent those variables with Diff_{st} between sites above 1.**

Variables	All periods		May - September		May - September Daytime	
	Diff_{st}	n	Diff_{st}	n	Diff_{st}	n
$\text{CO}_2, 0.05\text{m}$ (ppm)	-0.4027*	46340	-0.6578*	21413	-1.1396*	9816
$\text{CO}_2, 1.50\text{m}$ (ppm)	1.1196*	50133	1.3517*	24347	1.3062*	11385
$T_{0.05\text{m}}$ ($^{\circ}\text{C}$)	0.0927*	46337	-0.1160*	21410	-0.2119*	9813
$T_{1.50\text{m}}$ ($^{\circ}\text{C}$)	0.1476*	50137	-0.0591*	24350	-0.0834*	11385
$\text{VWC}_{0.05\text{m}}$ ($\text{m}^3 \text{m}^{-3}$)	0.8265*	52353	1.2724*	25231	1.2839*	11303
$\text{VWC}_{1.50\text{m}}$ ($\text{m}^3 \text{m}^{-3}$)	-0.8385*	53865	0.0674*	24570	0.0547*	11462

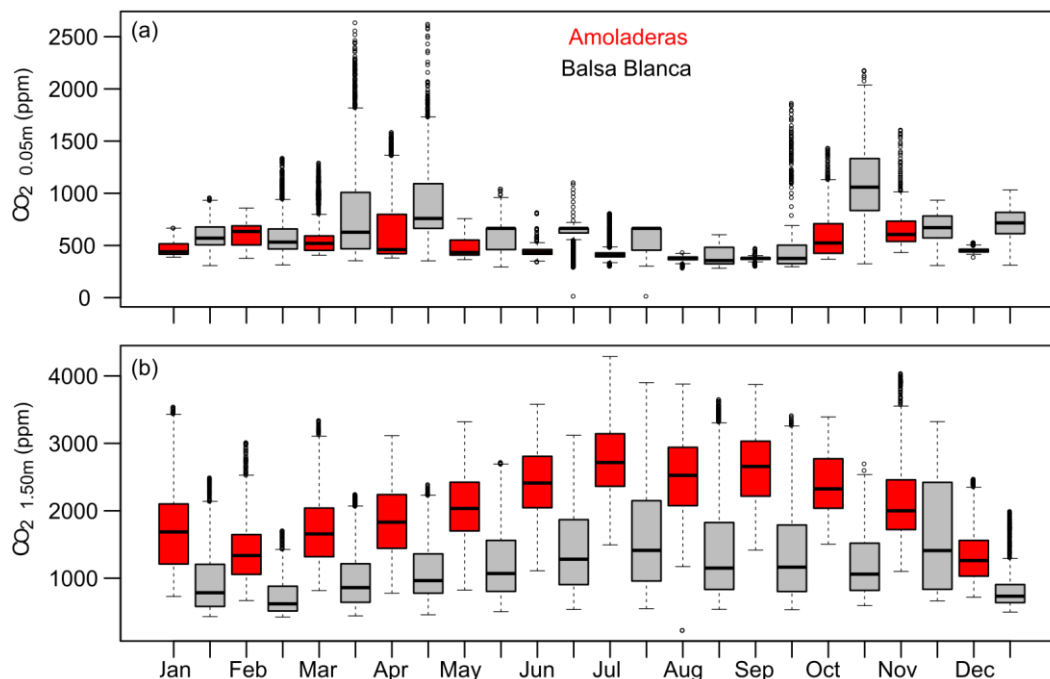


Figure 6: Box-and-whisker plots of CO₂ molar fractions measured at (a) 0.05 m and (b) 1.50 m belowground in Amoladeras (red boxes) and Balsa Blanca (grey boxes) from January 2014 to August 2015. The box extends from the first (Q1) to the third quartiles (Q3) and the central line represents the median (50% percentile). Dots represent outliers; upper whisker is located at the smaller of the maximum value and Q3 + 1.5 IQR (Interquartile Range), and lower whisker is located at the larger of the minimum value and Q1 – 1.5 IQR.

Table 6: Spearman correlation coefficients (r_s) for every paired simple correlation among maximum quality net CO₂ exchange fluxes ($\mu\text{mol m}^{-2} \text{s}^{-1}$), absolute and differential pressure (hPa) at 6, 12, 24 and 72 hours time-step and absolute and differential CO₂ molar fraction measured at 1.50 m below ground (ppm) at the same time-steps. Bold values represent the highest correlation coefficients while shaded ones denotes non-significant relationships (p-value>0.05).

	Amoladeras					Balsa Blanca				
	P	dP _{6h}	dP _{12h}	dP _{24h}	dP _{72h}	P	dP _{6h}	dP _{12h}	dP _{24h}	dP _{72h}
CO _{2, 1.50m}	-0.66	-0.33	-0.46	-0.56	-0.55	-0.33	-0.51	-0.53	-0.62	-0.45
dCO _{2, 1.50m_6h}	-0.1	-0.84	-0.5	-0.26	-0.01	-0.07	-0.63	-0.19	-0.13	-0.04
dCO _{2, 1.50m_12h}	-0.08	-0.57	-0.87	-0.55	-0.05	-0.03	-0.46	-0.50	-0.31	-0.03
dCO _{2, 1.50m_24h}	-0.13	-0.47	-0.78	-0.85	-0.15	-0.04	-0.40	-0.59	-0.58	-0.04
dCO _{2, 1.50m_72h}	-0.28	-0.28	-0.49	-0.64	-0.74	-0.13	-0.28	-0.43	-0.57	-0.48